Pyramidal pits created by single highly charged ions in BaF_2 single crystals

A. S. El-Said,[1,2,*] R. Heller,[1] F. Aumayr,[3] and S. Facsko[1]
[1]*Institute of Ion Beam Physics and Materials Research, Forschungszentrum Dresden-Rossendorf, Bautzner Landstr. 400, 01328 Dresden, Germany*
[2]*Physics Department, Faculty of Science, Mansoura University, 35516 Mansoura, Egypt*
[3]*Institute of Applied Physics, Vienna University of Technology, 1040 Vienna, Austria*
(Received 23 April 2010; published 9 July 2010)

In various insulators, the impact of individual slow highly charged ions (eV-keV) creates surface nanostructures, whose size depends on the deposited potential energy. Here we report on the damage created on a cleaved BaF_2 (111) surface by irradiation with $4.5\times q$ keV highly charged xenon ions from a room-temperature electron-beam ion trap. Up to charge states $q=36$, no surface topographic changes on the BaF_2 surface are observed by scanning force microscopy. The hidden stored damage, however, can be made visible using the technique of selective chemical etching. Each individual ion impact develops into a pyramidal etch pits, as can be concluded from a comparison of the areal density of observed etch pits with the applied ion fluence (typically 10^8 ions/cm^2). The dimensional analysis of the measured pits reveals the significance of the deposited potential energy in the creation of lattice distortions/defects in BaF_2.

DOI: 10.1103/PhysRevB.82.033403 PACS number(s): 61.80.Jh, 34.35.+a, 61.72.J−, 68.37.Ps

Swift heavy ions (MeV-GeV kinetic energy) have become an important tool for structural modifications of various materials at the microscale and nanoscale for a wide range of applications in the last two decades.[1–4] One major limitation of using these high-energy ions is the damage creation in deep layers which in some applications should be avoided. The desire to confine the damage to the first few layers, which is essential for applications such as ion projection lithography, has stimulated the interest for the use of slow (eV-keV) highly charged ions (HCIs).[5] This type of ions is now readily available after recent developments in ion source technology leading to powerful ion sources such as the electron-beam ion trap (EBIT).[6,7] While electronic energy loss of swift heavy ions is the major cause of material modifications,[8,9] potential-energy deposition is dominating surface modifications by HCI.[10] During interaction with the solid surface HCI deposit their potential energy (the total ionization energy required for producing the high charge state from its neutral ground state) within a few femtosecond in a nanometer-sized volume close to the surface.[10–12] Initially the potential energy is deposited in the electronic subsystem of the target leading to strong electronic excitations. Strong electron-phonon coupling can then induce local surface modifications in various solids. Recently, HCI-induced surface modifications such as hillocks,[13–15] craters,[16] pits,[17] and calderalike structures[18] with nanometer dimensions have been demonstrated.[10]

The study of nanostructure formation on surfaces induced by HCI is a relatively new field and still requires a detailed comparison between materials with common and different properties, in order to develop a more general understanding of the underlying mechanisms. For this aim and motivated by our recent findings regarding surface nanostructuring of CaF_2 by means of HCI (Refs. 13 and 14), we selected BaF_2 as one of the ionic alkaline-earth fluorides (along with CaF_2 and SrF_2) which have a wide range of potential applications in microelectronic and optoelectronic devices such as high-k dielectrics and buffer layers in semiconductor-on-insulator structures.[19]

As samples for irradiation, we have used thin slabs ($10\times10\times0.5-1.0$ mm^3) cleaved along the (111) planes from single-crystal blocks of high-purity barium fluoride (from Korth Kristalle, Germany) grown from melt in an inert atmosphere. The samples were mounted in a vacuum chamber with base pressure of 10^{-9} mbar and irradiated at room temperature under normal incidence with highly charged isotope pure $^{129}Xe^{q+}$ ions of various charge states ($q=24-36$). A rectangular transmission electron microscopy grid was used to mask parts of the sample surface. The ions were extracted from the EBIT in pulsed mode at constant extraction voltage of 4.5 kV leading to kinetic energies of $4.5\times q$ keV. The selection of ions of specific charge-to-mass ratio was performed using a 90 analyzing magnet. The applied ion fluences were in the range of 10^9-10^{10} ions/cm^2 whereas etching experiments required lower fluence of about 10^8 ions/cm^2, which is small enough to avoid tracks overlapping and reasonably high for good statistics. The average beam flux varied between 10^4 and 10^6 ions/s. Irradiation parameters are listed in Table I (some of the ion parameters are estimated using SRIM 2008).[20]

After ion irradiation, the BaF_2 (111) crystal surfaces were inspected by scanning force microscopy (SFM). The measurements were performed in tapping mode under ambient conditions using Si sensors (cantilever resonance frequency $\approx$190 kHz). Additionally, we performed UHV-contact mode SFM measurements (using UHV Omicron AFM/STM) at constant force and Si tips with cantilever force constants of $\approx$0.2 N/m. Surprisingly, none of the used Xe^{q+} ($q=24-36$) ions were able to induce visible topographic changes on the irradiated surfaces. As a typical example, Fig. 1 shows the SFM topographic image of a BaF_2 surface irradiated with 1.26 keV/amu Xe^{36+} ions. The peak-to-peak roughness of the cleaved surfaces is $\approx$0.1 nm which would be enough for resolving ion-induced surface structures of sizes above the SFM detection limit ($\approx$0.1 nm and 1.0 nm for vertical and lateral dimensions, respectively).

To reveal the hidden damage not directly visible in the

TABLE I. Charge state (q), potential energy (E_{pot}), kinetic energy (E_{kin}), and the corresponding electronic $(dE/dx)_e$, and nuclear $(dE/dx)_n$ energy loss, range (R) of the Xe ions as well as the mean measured depth (D) of the etch pits.

q	E_{pot} (keV)	E_{kin} (keV/amu)	$(dE/dx)_e$ (keV/nm)	$(dE/dx)_n$ (keV/nm)	R (nm)	D (nm)
24+	7.3	0.84	0.30	2.36	39	16
28+	12.0	0.98	0.32	2.39	44	19
33+	21.2	1.16	0.35	2.42	51	22
36+	27.8	1.26	0.37	2.44	54	23

surface topography, chemical etching was performed using a 1 vol % solution of HNO_3 at room temperature without agitation. To avoid any possible size dependence on etching time, all samples were etched under identical conditions (i.e., same HNO_3 concentration, 5 s etching time). Because parts of the sample's surface were masked by a rectangular copper grid during irradiation, the observation of well-defined patterns is a straightforward evidence of successful chemical etching of damage induced by HCI projectiles. Moreover, one can easily differentiate between features created due to ion irradiation and naturally present dislocations which are also etchable.[21]

In Fig. 2(a), the SFM topographic image of a BaF_2 surface irradiated with 10^8 Xe^{36+} ions/cm^2 is shown after chemical etching. Due to the pattern of the used rectangular mask irradiated and masked regions can be clearly distinguished. In irradiated areas, etch pits of three-faced symmetric pyramidal depressions are revealed. This geometry originates from the (111) crystal lattice orientation of BaF_2. The mean width and depth of the created etch pits are about 1.6 μm and 23 nm, respectively. In nonirradiated regions, etched surfaces only occasionally show a few pits as a result of etching naturally present dislocations, whose size, however, is much larger than the one observed for etched ion tracks [Fig. 2(a)].

Figures 2(b)–2(d) shows further SFM images of BaF_2 samples etched after irradiation with $(4.5q \times \text{kV})$ Xe^{24+}, Xe^{28+}, and Xe^{33+}, respectively. In all cases, triangle-shaped etch pits were observed in the irradiated areas whose sizes increase with the incident ion charge state and whose number corresponds to the applied ion fluence. Figure 3 shows a magnified image and a line profile through one of the pits.

Table I summarizes the parameters of our irradiation experiments including the electronic energy loss, the nuclear energy loss, and the penetration depth calculated by SRIM.[20] The potential energy corresponding to the lowest (Xe^{24+}) and highest (Xe^{36+}) charge state used in our experiments differ by a factor of 3.8. In contrast to this, the difference in the kinetic energy is only a factor of 1.5 leading to a difference of only 25% in the electronic energy loss and an insignificant difference of 3% in the nuclear energy loss. However, at these low kinetic energies the electronic energy loss is already one order of magnitude smaller than the nuclear energy loss. Taking into account that the potential energy is deposited within the first few nanometer,[14] the dominant role of the potential energy for the damage creation becomes obvious.

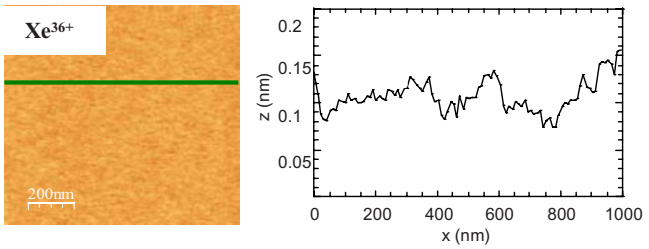

FIG. 1. (Color online) SFM topographic image and line scan of a BaF_2 (111) surface irradiated with 1.26 keV/amu Xe^{36+} ions (fluence 5×10^9 ions/cm^2). No topographic changes due to ion impact are visible.

In Fig. 4, the strong dependence of the mean size of the pits on potential energy is shown. The pit size is extracted from the SFM images by analyzing the width and depth of well-separated pits and calculating the removed volume (see Fig. 3). We note a nearly linear increase in pit volume with potential energy.

Before we interpret our findings for BaF_2 (111), we first compare them to results obtained during HCI irradiation of KBr (001) and CaF_2 (111) surfaces. For KBr (001) surfaces, the individual impacts of slow highly charged Xe ions induce nanometer-sized pitlike structures with lateral sizes of 10–25 nm and monatomic depth, which are visible in SFM without chemical etching.[17] For CaF_2 (111) surfaces, no topographic changes are visible in the SFM images up to a certain Xe-ion charge state ($q \leq 28$) while above this threshold permanent nanosized hillocks with lateral sizes of 20–40 nm and 0.5–1.0 nm height appear on the surface.[13,14] On the contrary, for BaF_2 (111) surfaces no topographic changes are visible in the SFM images up to the highest Xe-ion charge state ($q=36$) used in our experiments (see Fig. 1). Nanostructures in the form of pyramidal pits can, however, be revealed after chemical etching. All three cases have in common, that the nanostructures can unambiguously be associated to individual ion impact events and that the size of the generated nanostructures strongly depends on the charge state and therefore on the potential energy deposited by the HCI into the surface.[13,14,17]

The decisive role of the potential energy for the formation of nanostructures can be explained taking into account the fact that damage creation in ion-surface collisions is strongly correlated with the form of energy deposition in the solid. For slow (keV) singly charged or neutral atoms, nuclear stopping dominates the energy loss. This energy transfer to

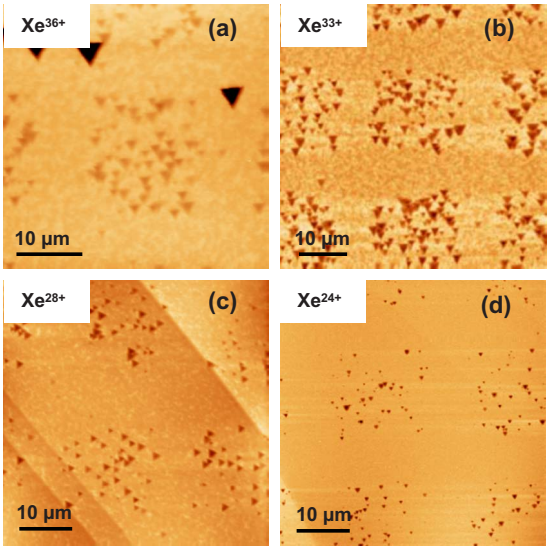

FIG. 2. (Color online) Scanning force micrographs of BaF_2 (111) surfaces after chemical etching. The samples were irradiated through a structured mask with (a) 4.5 keV/q Xe^{36+}, (b) Xe^{33+}, (c) Xe^{28+}, and (d) Xe^{24+} ions, respectively (fluence $\approx 10^8$ ions/cm^2).

target cores leads to atomic displacements and lattice vibrations in the target (phonons). On the other hand, slow highly charged ions transfer their potential energy via a series of Auger processes to the electronic subsystem of the target.[10–12] As a consequence, (i) a large number of electrons is emitted from the projectile into a shallow region close to the HCI impact zone,[22–24] (ii) inelastic interaction of these electrons with target atoms leads to a strong electronic excitation of a nanometer-sized region around the impact site,[10,11,25] i.e., generation of defects such as excitons, color centers, holes, etc., and production of further (secondary) electrons, and (iii) elastic collisions of these electrons with target atoms (electron-phonon coupling) heat the lattice in the surrounding of the impact site.

Modeling calculations for HCI impact on CaF_2 have shown that above a certain potential-energy threshold, the heating of the lattice atoms by these primary and secondary electrons can surpass the melting threshold of the solid.[14,26] Heat and pressure deforms the surface and after cooling

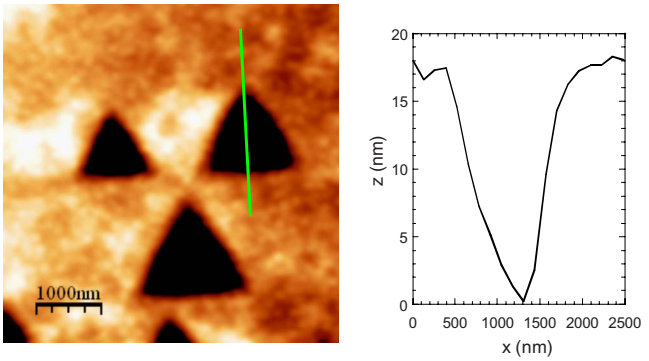

FIG. 3. (Color online) SFM image (left) of etched 4.5q ×keV Xe^{28+} pits in BaF_2 (111). Line profile across one of the pits (right).

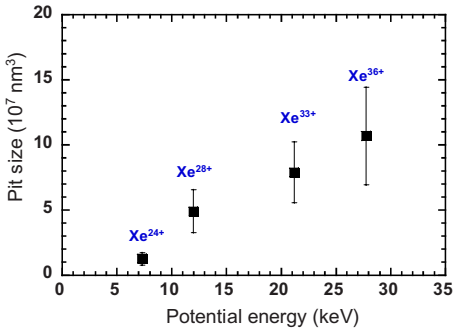

FIG. 4. (Color online) Mean size of etch pits as a function of potential energy of Xe^{q+} ions.

down a hillock remains at the surface. This melting threshold is obviously not (yet) reached for impact of Xe^{36+} on KBr and BaF_2. Since the melting temperatures are very similar in the case of CaF_2 and BaF_2 there have to be other reasons for this, which we can only speculate on (a) electron-transport properties, such as elastic and inelastic mean-free path could be different for both materials and transport the (electron) energy further away in the case of BaF_2 (resulting in a lower energy transferred to each target atom) (b) thermal conductivity of BaF_2 is higher than for CaF_2. So even if the same volume is heated by the electrons, this heat is more quickly carried away by heat conductivity or the hot zone is more effectively cooled from the surrounding material and therefore the zone does not melt. However, the strong electronic excitation will definitely lead to the generation of defects such as excitons, holes, color centers, etc., around the impact site also in these materials.

It is well known that even electron and photon impact on various ionic crystals can lead to color center creation and in further consequence to what is called electron- and photon-stimulated desorption.[27–29] The first steps include the production of holes and electron pairs. Because of the strong electron-phonon coupling of the ionic lattice, these defects become rapidly self-trapped (self-trapped exciton, self-trapped holes) (Refs. 30 and 31) and subsequently decay into color centers, i.e., an H center (an interstitial molecular halide ion) and an F center (an electron at an anion site). The independent diffusion of both centers and their subsequent recombination with the surface lead to the desorption of individual halide atoms and alkali (alkaline-earth) atoms, respectively.

This defect-induced desorption mechanism was also invoked to explain the interaction of singly[29] and multiply charged ions[11] with alkali-halide surfaces, in particular, to explain the effect of "potential sputtering," i.e., sputtering due to the potential energy of the projectile ions rather than their kinetic energy.[11,32–34] Also the pit formation during the interaction of HCI with KBr (001) (see above) was ascribed to this defect-induced desorption mechanism.[17] Contrary to the case of electrons, photons, or singly charged ions, however, the emission of a large number of electrons during the relaxation of HCI leads to a high density of defects close to the surface. As the defects diffuse, they combine to complex defect centers (e.g., F center agglomerates) from which in the case of KBr desorption is possible without the presence of step edges.[17]

As mentioned above, there is no reason to assume that the strong electronic excitation of the surface-near region due to the potential energy of the slow HCI should not induce similar defects and defect aggregates in BaF_2 and CaF_2 as well. However, in both cases the defects (or defect clusters) obviously do not result in pits visible in SFM images either because their diffusion is limited or the color centers remain (weakly) bound to the surface and do not lead to desorption. The impact region is, however, structurally weakened and can be preferentially attacked by a suitable etchant (as observed in our case for BaF_2).

In etching studies of swift heavy-ion tracks in alkali-halide surfaces, it was found that the etchability is related to the creation of large defect aggregates or even microdefects (clusters of few F centers) rather than single point defects (F and H centers).[35] The strong dependence of the mean size of etch pits as a function of potential energy of Xe^{q+} ions (Fig. 4) indicates that the electronic excitation induced by the HCI is able to create large defect aggregates at or close to the surface. Compared to the total ion range, the etch pits are only ≈40% deep (see Table I). This is a further hint that only in the beginning of the track (where the potential energy is deposited), etchable defect aggregates and clusters are produced while at the end of the ion track, point defects from the nuclear collision cascade prevail.

If our interpretation is correct, we should also be able to see similar structures after etching on CaF_2 (111) even below the (melting) threshold for hillock generation (see above). Indeed such etch pits have been found recently in preliminary experiments using Xe^{25+} projectile ion impact on CaF_2.[36] A more systematic study is currently in progress.

In conclusion, we have shown that in spite of no direct visible topographic surface modifications by HCI irradiation, surface and near surface lattice distortion are created in BaF_2 (111). The size of the revealed damage zone is strongly increasing with the deposited potential energy. The irradiation with slow HCI results in an extremely high and strongly localized dose distribution around the impact site. The etchability of the HCI-induced damage, suggests the efficient role of the deposited potential energy for the creation of defect aggregates rather than single point defects, an observation already made during swift heavy-ion irradiation.

A.S.E. thanks Alexander von Humboldt Foundation for financial support. This work was supported by the European project ITSLEIF (Grant No. RII3/026015).

*a.s.el-said@fzd.de; www.fzd.de

[1] M. Lang, F. X. Zhang, J. M. Zhang, J. Wang, B. Schuster, C. Trautmann, R. Neumann, U. Becker, and R. C. Ewing, Nature Mater. **8**, 793 (2009).
[2] A. Navitski, G. Mueller, V. Sakharuk, T. W. Cornelius, C. Trautmann, and S. Karim, Eur. Phys. J.: Appl. Phys. **48**, 30502 (2009).
[3] E. Akcöltekin, T. Peters, R. Meyer, A. Duvenbeck, M. Klusmann, I. Monnet, H. Lebius, and M. Schleberger, Nat. Nanotechnol. **2**, 290 (2007).
[4] T. W. Cornelius, J. Brötz, N. Chtanko, D. Dobrev, G. Miehe, R. Neumann, and M. E. T. Mollares, Nanotechnology **16**, S246 (2005).
[5] J. D. Gillaspy, D. C. Parks, and L. P. Ratliff, J. Vac. Sci. Technol. B **16**, 3294 (1998).
[6] F. Grossmann *et al.*, Nucl. Instrum. Methods Phys. Res. B **256**, 565 (2007).
[7] W. Meissl *et al.*, Rev. Sci. Instrum. **77**, 093303 (2006).
[8] A. S. El-Said *et al.*, Nucl. Instrum. Methods Phys. Res. B **256**, 313 (2007).
[9] K. Schwartz *et al.*, Phys. Rev. B **70**, 184104 (2004).
[10] F. Aumayr, A. S. El-Said, and W. Meissl, Nucl. Instrum. Methods Phys. Res. B **266**, 2729 (2008).
[11] F. Aumayr and H. P. Winter, Philos. Trans. R. Soc. London **362**, 77 (2004).
[12] T. Schenkel, A. V. Hamza, A. V. Barnes, and D. H. Schneider, Prog. Surf. Sci. **61**, 23 (1999).
[13] A. S. El-Said *et al.*, Nucl. Instrum. Methods Phys. Res. B **258**, 167 (2007).
[14] A. S. El-Said *et al.*, Phys. Rev. Lett. **100**, 237601 (2008).
[15] M. Terada *et al.*, Nucl. Instrum. Methods Phys. Res. B **235**, 452 (2005).
[16] M. Tona *et al.*, Surf. Sci. **601**, 723 (2007).
[17] R. Heller, S. Facsko, R. A. Wilhelm, and W. Moller, Phys. Rev. Lett. **101**, 096102 (2008).
[18] M. Tona *et al.*, J. Phys.: Conf. Ser. **58**, 331 (2007).
[19] M. Cao, C. Hu, and E. Wang, J. Am. Chem. Soc. **125**, 11196 (2003).
[20] J. F. Ziegler, P. Biersack, and U. Littmark, *The Stopping and Ranges of Ions in Solids* (Pergamon Press, Oxford, 1985).
[21] A. R. Patel and R. P. Singh, Jpn. J. Appl. Phys. **6**, 938 (1967).
[22] A. Arnau *et al.*, Surf. Sci. Rep. **27**, 113 (1997).
[23] H. P. Winter and F. Aumayr, J. Phys. B **32**, R39 (1999).
[24] F. Aumayr and H. P. Winter, Springer Tracts Mod. Phys. **225**, 79 (2007).
[25] S. Facsko, R. Heller, A. S. El-Said, W. Meissl, and F. Aumayr, J. Phys.: Condens. Matter **21**, 224012 (2009).
[26] C. Lemell *et al.*, Solid-State Electron. **51**, 1398 (2007).
[27] R. F. Haglund, Jr. *et al.*, Nucl. Instrum. Methods Phys. Res. B **13**, 525 (1986).
[28] M. Szymonski *et al.*, Surf. Sci. **260**, 295 (1992).
[29] N. Seifert *et al.*, Nucl. Instrum. Methods Phys. Res. B **101**, 131 (1995).
[30] R. T. Williams, K. S. Song, W. L. Faust, and C. H. Leung, Phys. Rev. B **33**, 7232 (1986).
[31] B. Such *et al.*, Phys. Rev. Lett. **85**, 2621 (2000).
[32] T. Neidhart, F. Pichler, F. Aumayr, HP. Winter, M. Schmid, and P. Varga, Phys. Rev. Lett. **74**, 5280 (1995).
[33] M. Sporn *et al.*, Phys. Rev. Lett. **79**, 945 (1997).
[34] G. Hayderer *et al.*, Phys. Rev. Lett. **86**, 3530 (2001).
[35] C. Trautmann, K. Schwartz, and O. Geiss, J. Appl. Phys. **83**, 3560 (1998).
[36] A. S. El-Said *et al.* (unpublished).